Chinese Journal of Natural Medicines

Gambogic acid suppresses pancreatic fibrosis *via* inhibiting YAP1-mediated activation of pancreatic stellate cells

Wei Li, Guangming Li, Yi Wang, Yuxin Zhou

Citation: Wei Li, Guangming Li, Yi Wang, Yuxin Zhou, Gambogic acid suppresses pancreatic fibrosis *via* inhibiting YAP1-mediated activation of pancreatic stellate cells, Chinese Journal of Natural Medicines, 2026, 24(1), 89-99. doi: 10.1016/S1875-5364(26)61079-5.

View online: https://doi.org/10.1016/S1875-5364(26)61079-5

Chinese Journal of Natural Medicines 24 (2026) 89-99

Contents lists available at ScienceDirect

Chinese Journal of Natural Medicines

journal homepage: www.cjnmcpu.com/

Original article

Gambogic acid suppresses pancreatic fibrosis *via* inhibiting YAP1-mediated activation of pancreatic stellate cells

Wei Li[a,Δ], Guangming Li[b,Δ], Yi Wang[b], Yuxin Zhou[b,*]

[a] *School of Integrated Chinese and Western Medicine, Nanjing University of Chinese Medicine, Nanjing 210023, China*
[b] *State Key Laboratory of Natural Medicines, Jiangsu Key Laboratory of Carcinogenesis and Intervention, China Pharmaceutical University, Nanjing 210009, China*

ARTICLE INFO

Article history:
Received 31 January 2025
Revised 11 April 2025
Accepted 17 June 2025
Available online 20 January 2026

Keywords:
Pancreatic fibrosis
Pancreatic stellate cells
Gambogic acid
YAP1

ABSTRACT

The activation of pancreatic stellate cells (PSCs) and the secretion of inflammatory factors play critical roles in the development of pancreatic fibrosis. While gambogic acid (GA), a flavonoid with anti-tumor properties, has been studied, its role in this process remains unclear. This study demonstrated that GA promoted YAP1 degradation and reduced its nuclear localization, thereby inhibiting PSC activation and the progression of pancreatic fibrosis. GA inhibited PSC proliferation, decreased *α*-smooth muscle actin (*α*-SMA) expression, and reduced lipid droplets in LTC14 and primary mouse PSCs (mPSCs). Additionally, GA suppressed the expression of inflammatory factors [nucleotide-binding oligomerization domain-like receptor protein 3 (NLRP3), nuclear factor erythroid 2-related factor 2 (NRF2), interleukin-6 (IL-6), tumor necrosis factor α (TNF-α), and nuclear factor *κ*B (NF-*κ*B)] in PSCs and counteracted the transforming growth factor (TGF)-β-induced increase in these proteins. GA also reduced collagen I and tissue inhibitor of metalloproteinase-1 (TIMP1) expression, thereby attenuating fibrosis. Mechanistically, GA decreased YAP1 expression and nuclear translocation and reversed TGF-β-induced YAP1 upregulation. YAP1 overexpression abrogated GA's inhibitory effects on PSC activation and inflammation. Furthermore, GA activated the Hippo pathway, increased phosphorylated (p)-LATS1 and p-YAP levels, and promoted ubiquitin-mediated YAP1 degradation. *In vivo* studies confirmed that GA inhibited dibutyltin dichloride (DBTC)-induced pancreatic fibrosis *via* suppressing YAP1 and NF-*κ*B in BALB/c mice. In conclusion, GA activates the Hippo pathway and promotes YAP1 translocation to the cytoplasm, leading to its degradation and subsequent inhibition of PSC activation and fibrosis. These findings highlight the critical role of ubiquitin-mediated YAP1 degradation in regulating PSC activity and offer novel insights into the therapeutic potential of GA for treating pancreatic fibrosis.

1. Introduction

Chronic pancreatitis (CP) is a progressive inflammatory disease of the pancreas, triggered by genetic predisposition, environmental exposures, and other contributing factors [1]. The condition is characterized by inflammatory cell infiltration, acinar cell atrophy, parenchymal fibrosis, pancreatic duct stenosis or dilation, and pancreatic duct stones [1, 2]. Recurrent acute injury primarily causes CP, resulting in scarring, remodeling, fibrosis, and calcification of the pancreas [1, 2]. Among these pathological changes, pancreatic fibrosis—characterized by excessive deposition of extracellular matrix (ECM) components—is a defining feature of CP and represents a major therapeutic challenge [3]. Fibrosis arises from an imbalance between ECM synthesis and degradation, leading to progressive replacement of functional parenchyma with rigid, fibrotic tissue. This process increases tissue stiffness, disrupts pancreatic architecture, and impairs both exocrine and endocrine function [4, 5]. Under homeostatic conditions, fibroblasts synthesize and maintain the ECM, including basal levels of collagen. However, in response to pathological stimuli, fibroblasts secrete a range of pro-inflammatory mediators that perpetuate the fibrotic microenvironment, exacerbate the inflammatory response, and promote both the initiation and progression of pancreatic fibrosis [6, 7].

Pancreatic stellate cells (PSCs), a specific type of pancreatic fibroblast, are integrally connected to pancreatic fibrosis progression [8, 9]. PSCs exist in quiescent and activated states [10]. In normal conditions, PSCs maintain a quiescent, fat-storing phenotype and are sparsely distributed throughout the pancreas, comprising 4% of pancreatic cells. These cells contain abundant vitamin A lipid droplets and express intermediate filaments, including desmin and glial fibrillary acidic protein (GFAP) [8, 11]. Upon exposure to pathological stimuli, PSCs become activated, undergo transdifferentiation into myofibroblast-like cells, and exhibit profound phenotypic and functional changes. Activated PSCs are characterized by the loss of cytoplasmic lipid droplets, enhanced migratory and proliferative capacities, upregulated synthesis of ECM components, and increased secretion of pro-inflammatory cytokines and chemokines. A hallmark of their activation is the elevated expression of *α*-smooth muscle actin (*α*-SMA) protein [12, 13]. Substantial evidence indicates that pancreatic inflammation and fibrogenesis drive robust PSC activation and proliferation, which

* Corresponding author.
E-mail address: zyxspain@hotmail.com (Y. Zhou)
Δ These authors contributed equally to this work.

https://doi.org/10.1016/S1875-5364(26)61079-5

in turn exacerbate both inflammatory and fibrotic responses, establishing a feed-forward loop that sustains disease progression [14]. In the early stages of chronic pancreatitis (CP), acinar cell injury initiates the recruitment of inflammatory cells and the release of key profibrotic mediators, including transforming growth factor-β (TGF-β) and platelet-derived growth factor (PDGF), which are critical triggers for PSC activation [7, 15]. Additionally, activated PSCs themselves secrete connective tissue growth factor (CTGF) and PDGF, thereby reinforcing their own activation and perpetuating a positive feedback mechanism that accelerates the progression of pancreatic fibrosis [8].

The imbalance between pro-inflammatory and anti-inflammatory responses contributes to local tissue damage and organ injury. Given that activated PSCs play a central role in pancreatic fibrosis, inhibiting their activation and inflammatory factor secretion may help reduce fibrosis and treat CP [16]. Select phytochemicals targeting PSCs serve as novel anti-fibrotic agents for CP and pancreatic cancer. Curcumin suppresses PSC activation and migration *via* the interleukin-6 (IL-6)/ERK and nuclear factor κB (NF-κB) pathways, thereby decreasing fibrosis levels [17]. Puerarin inhibits PSC migration and activation through the MAPK pathway [18]. NF-κB is activated in early pancreatitis stages and regulates PSC inflammation, survival, proliferation, and migration [19, 20]. Mouse models demonstrate that increased NF-κB activity correlates with enhanced pancreatic fibrosis, while NF-κB knockout reduces fibrosis [20, 21]. Recent studies indicate that the Hippo-YAP1 signaling pathway as a key regulator of pancreatic fibrosis. In particular, the functional interplay between the Hippo pathway and the NF-κB signaling cascade has been shown to modulate PSC proliferation, activation, and fibrogenic activity [22, 23]. YAP1 may affect pancreatic fibrosis progression by promoting PSC activation and inflammatory response development. Multiple studies have confirmed that YAP1 directly influences the activation status of PSCs [24]. Xiao et al. found that YAP1 regulation affects PSC activation and paracrine function, potentially inhibiting pancreatic cancer development [25]. YAP1-TAZ interaction can inhibit cytoskeletal remodeling in PSCs, thus suppressing PSC proliferation and activation [26]. Additionally, YAP1 also plays a central role in inflammatory responses, and the Hippo-YAP1 signaling pathway interacts with various inflammatory factors [27]. The Hippo-YAP1 pathway intricately modulates NF-κB signaling as both a positive and a negative regulator. LPS stimulation promotes YAP1 and NF-κB interactions, while lactic acid disrupts their interaction and nuclear translocation in macrophages [28]. Endothelial-specific YAP1 knockout mice exhibit reduced NF-κB activity and decreased pro-inflammatory cytokine expression of IL-1, tumor necrosis factor α (TNF-α), and IL-6, resulting in reduced lung inflammation and mortality [29]. Moreover, Deng et al. demonstrated YAP1's suppression of NF-κB-mediated inflammatory responses in experimental osteoarthritis mouse models [30]. As a key regulator of PSC proliferation and inflammation, YAP1 represents a promising target for inhibiting pancreatic fibrosis.

Gamboge, indigenous to Southeast Asian countries, and its active component, gambogic acid (GA, $C_{38}H_{44}O_8$), have traditional applications in Chinese medicine and throughout Southeast Asia. Research indicates that GA effectively inhibits various tumors by promoting cancer cell apoptosis, suppressing cancer cell migration and invasion, inducing cell cycle arrest, inhibiting tumor angiogenesis, and regulating autophagy, establishing it as a promising natural compound. Wang et al. demonstrated that GA inhibits pancreatic cancer cell proliferation by suppressing transcription factor ETS-1 activity [31]. Furthermore, Saeed et al. identified GA's synergistic effect with chemotherapy drugs in pancreatic cancer treatment [32]. Studies show that GA inhibits hepatic and pulmonary fibrosis development [33, 34], though its specific role and mechanism in inhibiting PSC activation remain unclear. Additionally, pancreatic fibrosis contributes to the formation of a dense stromal barrier that significantly hinders the delivery and efficacy of chemotherapeutic agents. By mitigating fibrotic remodeling, GA may enhance drug penetration and improve the therapeutic response to agents such as gemcitabine. These findings suggest that GA holds potential as a stromal-targeting adjuvant, offering a promising strategy to augment chemotherapy efficacy and improve clinical outcomes in pancreatic cancer treatment.

2. Materials and methods

2.1. Cell lines and cell culture

Rat PSCs LTC14 and HPNE cells were obtained from the cell bank at the Shanghai Institute of Biochemistry and Cell Biology (Shanghai, China). Cells were cultured in RPMI-1640 medium (Cat. No. KGL1503-500, KeyGen BioTech, Nanjing, China) supplemented with 100 U·mL^{-1} penicillin (Sangon Biotech, Shanghai, China), streptomycin sulfate (Beyotime Biotechnology, Shanghai, China), and 10% FBS (Cat. No. RY-F22-01, Royacel Biotech, Lanzhou, China). Both cell lines were maintained at 37 °C in a humidified atmosphere with 5% CO_2. Passaging was performed using a mixture of EDTA buffer and 0.25% trypsin.

2.2. Animals

Female BALB/c mice (6–8 weeks old, weighing 20 ± 2 g) were obtained from Hangzhou Medical College [No. SCXK (ZHE)-2024-0002]. The mice were maintained in standard conditions (temperature: 25 ± 1 °C, humidity: 40%–60%, 12 h light/dark cycle) for 1 week prior to experimentation. All animal procedures adhered to ethical guidelines and were conducted using a double-blind approach (approval number: 202306A028).

2.3. Extraction of primary mouse PSCs (mPSCs)

Following euthanasia, mice were immersed in a 75% ethanol solution for 5 min. The pancreas was extracted under sterile conditions and placed in a petri dish. The tissue was washed three times with pre-cooled (4 °C) D-Hank's (Cat. No. KGL2201-500, KeyGen BioTech, Nanjing, China). The pancreatic tissue was cut into 1 mm^3 pieces in enzyme digestion solution (Cat. No. C917426, Macklin, Shanghai, China) and transferred to a 10 cm petri dish. After digestion at 37 °C for 30 min, the tissue was ground and filtered through a 70 μm sieve. Digestion was terminated by adding freshly prepared 3% bovine serum albumin (BSA) solution (Cat. No. 4240GR100, Biosharp, Hefei, China) or fetal bovine serum (Cat. No. RY-F22-01, Royacel Biotech, Lanzhou, China). The filtrate was centrifuged at 1200 r·min^{-1} for 10 min, and the supernatant was discarded. The collected cells were cultured at 37 °C until reaching 90% confluence before passaging. First-passage cells were used for experiments.

2.4. Reagents

GA ($C_{38}H_{44}O_8$, 98% purity) was synthesized and provided by Prof. Zhiyu Li (State Key Laboratory of Natural Medicines, Jiangsu Key Laboratory of Carcinogenesis and Intervention, China Pharmaceutical University). For *in vitro* experiments, GA was dissolved in dimethyl sulfoxide (DMSO, Cat. No. 472301, Merck, St. Louis, MO, USA) to 0.01 mol·L^{-1}, stored at −80 °C, and diluted as required. For *in vivo* experiments, GA was formulated for intragastric administration by Dr. Xue Ke from the College of Pharmacy, China Pharmaceutical University, and dissolved in sodium carboxymethyl cellulose (CMC-Na) to 80 mg·kg^{-1} before use.

DBTC ($C_8H_{18}C_{12}Sn$, ≥ 97% purity) was obtained from Shanghai Aladdin Biochemical Technology Co., Ltd. (Shanghai, China). DBTC was dissolved in anhydrous ethanol and glycerol (3∶2 ra-

tio) to 8 mg·kg^{-1} before use.

TGF-β (≥ 99% purity) was obtained from Merck (Cat. No. 5.08158, St. Louis, MO, USA).

2.5. Immunofluorescence (IF)

Harvested cells were washed twice with phosphate-buffered saline (PBS) before being spread onto glass slides. The cells were fixed with 4% polymethanol (Cat. No. 8.18715, Shanghai Lingfeng Chemical Reagent, Shanghai, China) for 10 min and permeabilized with 0.3% Triton X-100 (Cat. No. 1139ML100, Saiguo Biotech, Guangzhou, China) for 10 min. The cells were blocked with 3% BSA (Cat. No. 4240GR100, Biosharp, Hefei, China) for 2 h at room temperature. Subsequently, cells were incubated overnight with primary antibody (1∶100) at 4 °C, followed by incubation with fluorescent secondary antibody (1∶100) for 40 min at room temperature in darkness. The plates were treated with DAPI anti-quencher (Cat. No. C1006, Beyotime Biotechnology, Shanghai, China). Cell observation was performed using a laser scanning confocal microscope (Fluoview FV1000, Olympus, Tokyo, Japan).

2.6. Oil Red O staining

LTC14 and mPSCs underwent treatment with specified drugs/reagents at designated time points. The experiments were conducted using the Oil Red O staining kit (Cat. No. C0157S, Beyotime Biotechnology, Shanghai, China). The cells were fixed with 4% polymethanol for 10 min and rinsed with PBS at room temperature. Subsequently, cells were exposed to dye wash solution for 20 s and stained for 15 min at room temperature using 0.3% Oil Red O in 60% isopropyl alcohol, followed by PBS washing. Nuclear staining was performed using hematoxylin staining solution, and images were captured *via* inverted microscopy (DP72, Olympus, Tokyo, Japan).

2.7. Western blot and immunoprecipitation

Western blot and immunoprecipitation assays were performed as previously described [35]. Primary antibodies utilized in Western blot included *α*-SMA and NF-*κ*B (1∶1000, Cat. No. 14395-1-AP and 80979-1-RR, Proteintech, Wuhan, China), NLRP3, NRF2, IL-6, collagen I, *β*-actin and GAPDH (1∶1000, Cat. No. A12649, AP1133, A27935, A21059, AC028 and AC054, ABclonal, Wuhan, China), YAP1 and ubiquitin (1∶1000, Cat. No. YM8331 and YM9016, Immunoway Biotechnology, California, USA), TNF-α, MMP2, MMP3 and MMP9 (1∶1000, Cat No. RPH00477, RMAB49602, RMAB49604 and RMAB49605, Bioswap, Beijing, China), and TIMP1, MST1, LATS1, TAZ, p-LATS1 and p-YAP1 (1∶1000, Cat. No. FNab08706, FNab07384, P0732, P6182, P0732 and FNab09559, FineTest, Wuhan, Chian). Each blot represents one example from at least three repetitions.

2.8. ROS measurement

LTC14 and mPSCs were collected and stained using the ROS assay kit (Cat. No. S0034S, Beyotime Biotechnology, Shanghai, China) according to the manufacturer's protocols. The cells were then incubated with DCFH-DA dye, diluted in serum-free DMEM (Cat. No. KGM12800, KeyGEN Biotech, Nanjing, China) at 1∶1000, for 20 min at 37 °C in darkness. Flow cytometry (AccuriTM C6, BD, New Jersey, USA) and CellQuest software 3.0 were employed for data acquisition and analysis.

2.9. ELISA

IL-6 concentrations in cell supernatant were determined *via* ELISA following protocols (Cat. No. EM0004, Youke Life, Hangzhou, China). The coating antigen diluted in coating buffer was applied to a 96-well microplate (200 μL per well) and incubated overnight at 4 °C. After washing the plate three times with PBS with Tween-20 (PBST), blocking was performed using 1% casein (280 μL per well) for 1 h at room temperature. Following PBST washing, IL-6 standard (100 μL per well) and mAb solution (100 μL per well, diluted in PBS) were added and gently agitated for 1 h at room temperature. After three additional washes, HRP-GaMIgG solution (200 μL per well, diluted in PBS) was added and incubated for 1 h at room temperature. Following washing, the enzymatic substrate solution (200 μL per well) was added and incubated with gentle agitation for 15–20 min. The reaction was terminated using 5% sulfuric acid (80 μL per well), and absorbance measurements were taken at 450 nm using an ELISA reader.

2.10. Real-time PCR analysis

RNA was reversely transcribed to cDNA following the reverse transcription kit instructions (Cat. No. MR101-02, Vazyme Biotech, Nanjing, China). The reaction was prepared according to SYBR Green I reagent specifications (Cat. No. Q221-01, Vazyme Biotech, Nanjing, China), and PCR was performed using real-time qPCR (QuanStudio3, Applied Biosystems, Waltham, USA). Data were analyzed and exported using BIO-RAD CFX Maestro Software 2.3. The relative mRNA expressions were calculated using the $2^{-\Delta\Delta CT}$ method and normalized to *GAPDH*.

The primer sets used in the PCR assay are shown in Table S1.

2.11. Construction of stable transfected cells

Experiments were conducted following the lentivirus packaging kit protocol (Cat. No. 41102ES, Yeasen Biotechnology, Shanghai, China). LTC14 cells in logarithmic growth phase were seeded into six-well plates and packaged when cell adherence reached 80% confluence. Fresh medium was replaced 2 h beforehand. In a 200 μL preparation system, 2 μL viral plasmid, 2 μg target plasmid, and 60 μL Hg transgene transfection reagent were combined and incubated for 20 min. The mixture was added dropwise in a circular pattern onto the six-well plate. Fluorescence intensity was monitored after 24 h, and virus supernatant was collected *via* centrifugation at 48 h. The supernatant was filtered through a 0.22 μm filter tip and stored at −80 °C. For lentiviral infection, target cells were treated with virus supernatant and complete medium at a 1∶1 ratio. Polybrene was added to achieve a final concentration of 10 μmol·L^{-1}, followed by selection with 4 μg·mL^{-1} puromycin to obtain stably transfected cells.

2.12. Induction of CP in mice

Eighteen BALB/c mice were randomly assigned to three groups: control group, DBTC group, and DBTC + GA group. Pancreatitis was induced in BALB/c mice by administering DBTC (8 mg·kg^{-1} body weight) *via* tail vein injection on days 1, 8, and 15. GA (80 mg·kg^{-1}) was administered orally daily beginning on day 4. Blood samples were collected from the orbital sinus 24 h after initial DBTC administration and on day 28. Subsequently, mice were euthanized, and pancreatic tissue was harvested, washed, photographed, fixed, and embedded in paraffin for further analysis.

2.13. H&E staining

Following euthanasia, pancreatic tissue was surgically excised and fixed in 4% paraformaldehyde solution for 24 h. Samples were processed at the Pathology and PDX Pharmacology Evaluation Platform at China Pharmaceutical University for paraffin embedding and sectioning. H&E staining and slide analysis

were performed by the pharmacology platform. Stained sections were examined and photographed using a microscope (IX51, Olympus, Tokyo, Japan), with nuclei appearing blue and cytoplasm pink or red.

2.14. Masson staining

Masson staining and slide analysis were conducted by the Pathology and PDX Pharmacology Evaluation Platform at China Pharmaceutical University. Stained sections were examined and photographed under a microscope, revealing blue collagen fibers, mucus, and cartilage; red muscle fibers, fibrin, and red blood cells; and blue-black nuclei.

2.15. Serum α-amylase content measurement

Blood samples (approximately 500–1000 μL per mouse) were collected from the orbital sinus, maintained at room temperature for 30 min, and centrifuged at 4000 r·min^{-1} for 10 min. The supernatant was collected and stored at −20 °C. Serum α-amylase content was determined using the kit (Cat. No. 41102ES, Wuhan Seville Biotechnology, Wuhan, China).

2.16. Immunohistochemistry

Protein expression in pancreatic tissues was evaluated using the PV-9000 kit (Cat. No. PV-9000, Zhong Shan Golden Bridge Biological Technology, Beijing, China), following established protocols [33]. Pancreatic tissue sections (4 μm) were deparaffinized with xylene and rehydrated through graded alcohol solutions. Protein visualization employed the streptavidin peroxidase-conjugated method. Sections were incubated with primary antibodies targeting specific proteins: α-SMA, NK-κB (1∶1000, Cat. No. 14395-1-AP and 80979-1-RR, Proteintech, Wuhan, China), and YAP1 (1∶1000, Cat. No. YP0708, Immunoway Biotechnology, California, USA).

2.17. Statistical analysis

Data were expressed as mean ± SD. Group differences were analyzed using one-way analysis of variance (ANOVA) with IBM SPSS Statistics Software 18.0. Statistical significance was set at $P < 0.05$, with $P < 0.01$ indicating high significance. GraphPad Prism Software 8.0.2 was used for graphical representation.

3. Results

3.1. GA inhibits PSC proliferation and activation

We isolated mPSCs from mice and investigated the effects of GA on their proliferation and activation (Fig. 1A). Immunofluorescence (IF) results demonstrated that α-SMA protein expression was detected by day 6 (Fig. 1B). Oil Red O staining was conducted on primary mPSCs at days 3, 9, and 12. On day 3, mPSCs exhibited a spindle-shaped morphology with substantial accumulation of intracellular lipid droplets. By day 9, the cells transitioned to a multipolar morphology, accompanied by a marked reduction in lipid droplet content. By day 12, the cells had largely lost their spindle-shaped structure, appeared more dispersed, and displayed further depletion of lipid droplets (Fig. 1C). As illustrated in Fig. 1D, GA significantly inhibited the growth of LTC14 and mPSCs. The half maximal inhibitory concentration (IC_{50}) values of 24 h GA treatment for LTC14, mPSCs, and human pancreatic nestin-expressing (HPNE) cells were 0.74 ± 0.14, 0.74 ± 0.04, and 4.98 ± 0.38 μmol·L^{-1}, respectively. These findings demonstrated that GA exhibits selective activity between PSCs and HPNE cells at specific concentrations. The effects of GA on α-SMA expression in LTC14 and mPSCs were evaluated by Western blot and IF. As shown in Figs. 1E and 1F, 24 h GA treatment dose-dependently decreased α-SMA and reversed TGF-β-induced α-SMA expression. Oil Red O staining revealed that GA enhanced lipid droplets in LTC14 and mPSCs, while also preventing TGF-β-induced lipid droplet reduction (Figs. 1G and 1H). These results indicate that GA inhibits the activation of LTC14 and mPSCs.

3.2. GA inhibits inflammation and fibrosis-related proteins in PSCs

During PSC activation, ROS levels increase significantly. GA demonstrated the ability to reduce ROS levels in LTC14 and mPSCs (Fig. 2A). Activated PSCs release inflammatory factors that further promote inflammation development and subsequently intensify fibrosis [5, 6]. Western blot analysis demonstrated that GA significantly reduces the expression of nucleotide-binding oligomerization domain-like receptor protein 3 (NLRP3), nuclear factor erythroid 2-related factor 2 (NRF2), IL-6, TNF-α, and NF-κB, while reversing the TGF-β-induced elevation of these proteins (Figs. 2B and 2C). Furthermore, enzyme-linked immunosorbent assay (ELISA) analysis revealed that GA dose-dependently decreases IL-6 secretion in LTC14 cells and mPSCs (Fig. 2D). Activated PSCs produce ECM components, matrix metalloproteinases (MMPs), and their inhibitors [tissue inhibitor of metalloproteinases (TIMPs)]. An imbalance in MMP and TIMP expression levels represents a primary cause of ECM deposition [16]. Collagen I serves as a key effector molecule in fibrosis [36, 37]. Western blot analysis was used to detect the expression of collagen I, MMP2, MMP3, MMP9, and TIMP1. As shown in Fig. 2E, GA significantly decreased collagen I and TIMP1 levels, while dose-dependently increasing MMP2, MMP3, and MMP9 expression. To establish the causal relationship between reduced ROS levels, decreased inflammatory proteins, and improved fibrosis, an H_2O_2-induced cell model was employed to simulate oxidative stress conditions. Through analysis of changes in inflammatory factors (Fig. 2F) and fibrosis-related protein markers (Fig. 2G), the positive effect of GA-induced ROS reduction on fibrosis improvement was further confirmed. These results suggest that GA promotes ECM degradation and reduces fibrosis.

3.3. GA inhibits PSC activation by suppressing YAP1 expression and nuclear translocation

YAP1 demonstrates elevated expression in pancreatic cancer and CP patients, significantly affecting pancreatic fibrosis progression [26, 38, 39]. However, its precise role and mechanism in PSCs remain to be elucidated. As demonstrated in Fig. 3A, YAP1 expression in LTC14 and mPSCs exhibits significantly higher levels compared to HPNE cells. To investigate YAP1's function in PSCs, stable YAP1-overexpressing LTC14 cells were generated using lentivirus, while transient YAP1 overexpression in mPSCs was achieved using Lipo 2000. Control cells were transfected with an empty CMV plasmid. Western blot analysis confirmed the successful establishment of YAP1-overexpressing cells [designated as YAP1 complementary deoxyribonucleic acid (cDNA) in figures], enabling their use in subsequent experiments (Fig. 3B). MTT analysis revealed that the IC_{50} values of GA for YAP1-overexpressing LTC14 and mPSCs were 1.67 ± 0.14 and 1.45 ± 0.20 μmol·L^{-1}, respectively (Fig. 3C), notably higher than those observed in normal LTC14 and mPSCs. These findings indicate that YAP1 overexpression diminishes GA's inhibitory effect on PSC proliferation. As illustrated in Fig. 3D, 24-h GA treatment decreased YAP1 expression in LTC14 and mPSCs in a dose-dependent manner, while also counteracting the TGF-β-induced elevation in YAP1 expression. IF analysis further demonstrated that GA decreases YAP1 nuclear translocation in LTC14 and mPSCs

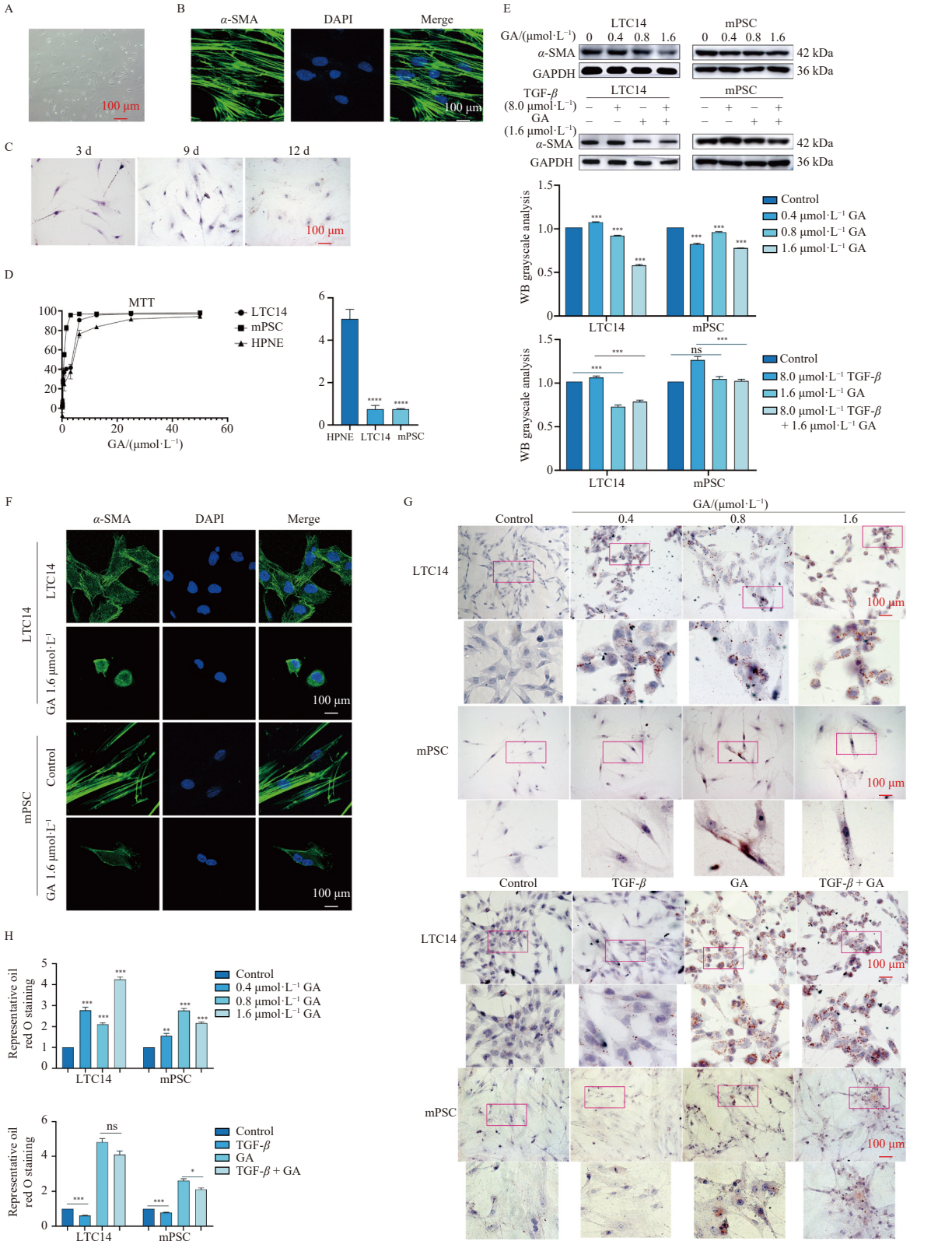

Fig. 1 The effects of GA on the proliferation and activation of PSCs. (A) Morphology of mPSCs (day 2): the cells had both round and spindle shapes. (B) On day 6, the IF assay detected SMA expression in mPSCs (scale bars, 100 μm). (C) The lipid droplets in mPSCs were detected by Oil Red O staining on days 3, 9, and 12 (scale bars, 100 μm). (D) MTT assay was used to detect the proliferation inhibition of GA (0–50 μmol·L^{-1}) on LTC14, mPSCs, and HPNE cells. (E) The effect of GA on α-SMA expression in LTC14 and mPSCs without/with 8 μmol·L^{-1} TGF-β was analyzed by Western blot. (F) The effect of GA on α-SMA protein expression in LTC14 and mPSCs was verified by IF (scale bars, 100 μm). (G and H) The effect of GA on lipid droplets in LTC14 and mPSCs without/with 8 μmol·L^{-1} TGF-β was detected by Oil Red O staining (scale bars, 100 μm). Data were expressed as mean ± SD (n = 3), $^{*}P < 0.05$, $^{**}P < 0.01$, $^{***}P < 0.001$, $^{****}P < 0.0001$ *vs* control group/specified group.

(Fig. 3E).

As demonstrated in Fig. 3F, YAP1 overexpression decreased lipid droplet formation, whereas GA treatment enhanced their formation in LTC14 and mPSCs. Furthermore, YAP1 overexpression attenuated the GA-induced increase in lipid droplets. The expression of α-SMA was enhanced in YAP1-overexpressing PSCs, while GA treatment markedly reduced α-SMA levels (Fig. 3G). These findings suggest that GA inhibits PSC activation through

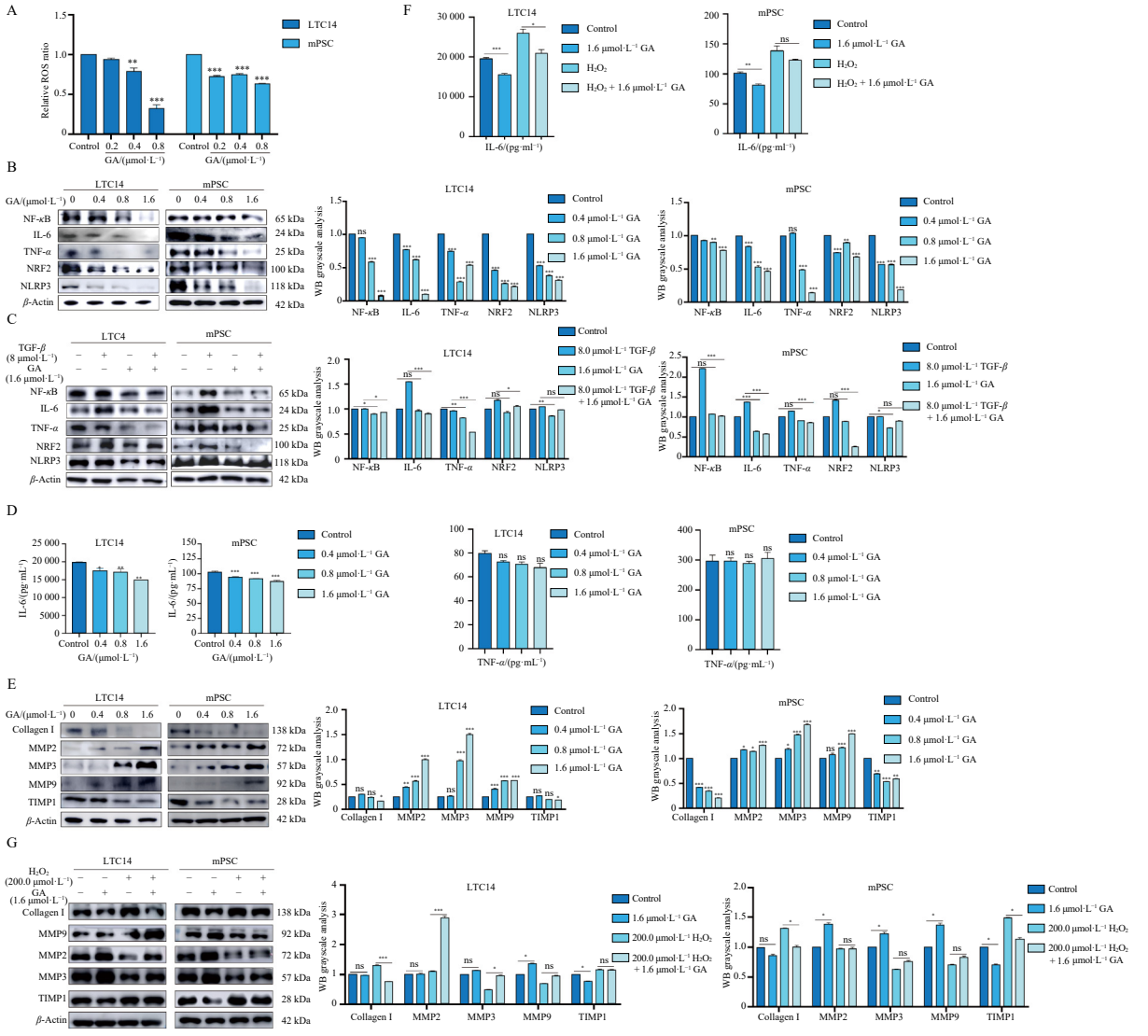

Fig. 2 The effect of GA on inflammation and fibrosis-related proteins in PSCs. (A) The effect of GA on ROS levels in LTC14 and mPSCs was measured by flow cytometry. (B) The effect of GA on inflammation-related protein (NLRP3, NRF2, IL-6, TNF-α, and NF-κB) in LTC14 and mPSCs was analyzed by Western blot. (C) The effect of GA on the TGF-β-induced increase in inflammation-related proteins in LTC14 and mPSCs was analyzed by Western blot. (D) The effect of GA on IL-6 and TNF-α in LTC14 and mPSCs was detected by ELISA. (E) The effect of GA on fibrosis-related protein expression (collagen I, MMP2, MMP3, MMP9, and TIMP1) in LTC14 and mPSCs. (F) The effect of H_2O_2 and/or GA on IL-6 in LTC14 and mPSCs was detected by ELISA. (G) The effect of H_2O_2 and/or GA on fibrosis-related protein expression (collagen I, MMP2, MMP3, MMP9, and TIMP1) was analyzed by Western blot. Data were expressed as mean ± SD (n = 3), $^{*}P < 0.05$, $^{**}P < 0.01$, $^{***}P < 0.001$, $^{****}P < 0.0001$ *vs* control group/specified group.

YAP1 suppression. YAP1 demonstrates interactions with immune factors, including NF-κB and NRF2, thereby influencing fibrosis through inflammatory response modulation [30, 40]. To investigate YAP1's role in GA-mediated inhibition of PSC inflammatory response, the expression levels of key inflammatory factors were analyzed. As illustrated in Fig. 3H, GA significantly reduced NF-κB, NRF2, IL-6, and TNF-α protein expression in PSCs, although YAP1 overexpression diminished these inhibitory effects. Western blot analysis of collagen I revealed that YAP1 overexpression counteracted the GA-induced decrease in collagen I (Fig. 3I). These results indicate that GA facilitates YAP1 translocation to the cytoplasm, resulting in its degradation and subsequent inhibition of PSC activation and fibrosis.

3.4. GA activates the Hippo pathway and promotes the degradation of YAP1

To determine whether GA regulates YAP1 through the Hippo pathway, Hippo pathway-related proteins were examined. As illustrated in Fig. 4A, GA treatment maintained MST1 expression levels while reducing LATS1 and TAZ expression and increasing phosphorylated (p)-LATS1 and p-YAP levels. Quantitative polymerase chain reaction (qPCR) analysis of Hippo pathway and downstream target gene transcription (Fig. 4B) revealed decreased messenger ribonucleic acid (mRNA) levels of *YAP1*, *TAZ*, *CTGF*, and *CYR61*, accompanied by increased *RASSF4* expression. These findings demonstrate that GA activates the Hippo pathway, resulting in LATS1 activation and elevated p-LATS1 and p-YAP levels.

Upon activation of the Hippo pathway, YAP1 undergoes transformation into p-YAP1 and accumulates in the cytoplasm, where it subsequently undergoes ubiquitination and degradation [41, 42]. Previous research demonstrates that GA treatment decreases YAP1 protein levels and facilitates its cytoplasmic translocation, indicating potential degradation outside the nucleus. To investigate this process, CHX was utilized to inhibit new protein synthesis while monitoring YAP1 protein degradation during GA treatment. YAP1 protein levels were assessed at 0, 3, 6, 12, and 24 h following GA treatment of PSCs to evaluate degradation rates. The findings demonstrate that GA enhances YAP1 degradation when protein synthesis is inhibited (Fig. 4C). Immunoprecipitation analysis revealed that GA strengthens the interaction between YAP1 and ubiquitin, indicating GA promotes YAP1 ubiquitination and subsequent degradation (Fig. 4D). Administra-

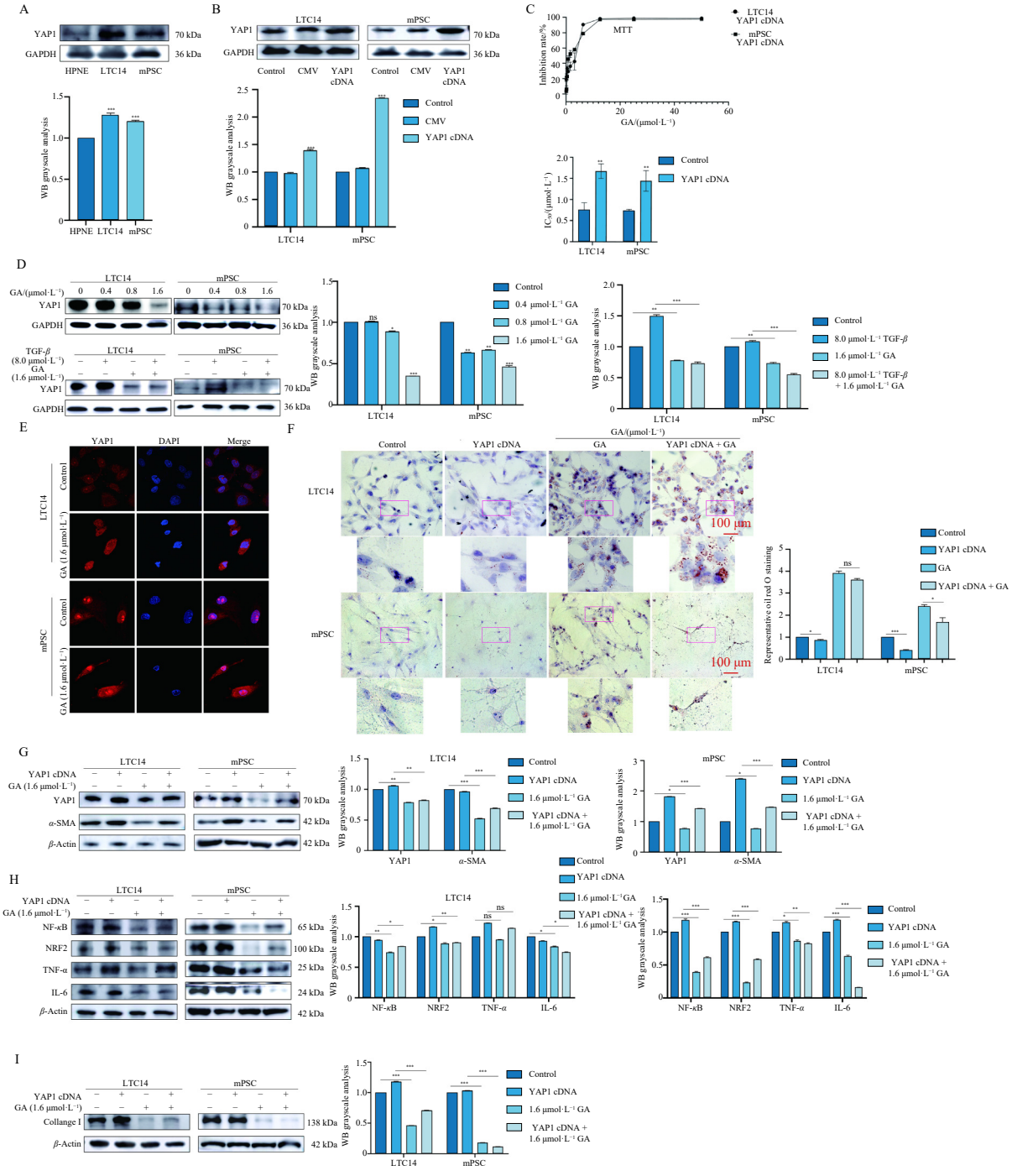

Fig. 3 The effect of GA on YAP1 expression and nuclear translocation. (A) The expression of YAP1 in HPNE cells, LTC14, and mPSCs was anlyzed by Western blot (an empty CMV plasmid served as control). (C) The inhibitory effect of GA (0−50 μmol·L^{-1}) on the proliferation of YAP1-overexpressing LTC14 and mPSCs was analyzed by MTT. (D) The effect of GA on YAP1 expression in LTC14 and mPSCs without/with 8 μmol·L^{-1} TGF-β was analyzed by Western blot. (E) The effect of GA on the localization of YAP1 in LTC14 and mPSCs was detected by IF. (F) The effect of GA on lipid droplets in YAP1-overexpressing LTC14 and mPSCs was detected by Oil Red O staining (scale bars, 100 μm). (G) The effect of GA on YAP1 and α-SMA expression in YAP1-overexpressing LTC14 and mPSCs was analyzed by Western blot. (H) The effect of GA on inflammation-related protein (NRF2, IL-6, TNF-α, and NF-κB) in YAP1-overexpressing LTC14 and mPSCs was analyzed by Western blot. (I) The effect of GA on Collange I in YAP1-overexpressing LTC14 and mPSCs was analyzed by Western blot. Data were expressed as mean ± SD (n = 3), $^{*}P < 0.05$, $^{**}P < 0.01$, $^{***}P < 0.001$, $^{****}P < 0.0001$ *vs* control group/specified group.

tion of the proteasome inhibitor MG132 reversed GA-induced YAP1 downregulation, confirming that GA facilitates YAP1 degradation through the ubiquitination-proteasome pathway (Fig. 4E). Additionally, GA treatment was observed to reduce NF-κB protein expression in LTC14 cells while enhancing YAP1 and NF-κB interaction (Fig. 4D). IF analysis (Fig. 4F) demonstrates that GA induces YAP1 translocation from the nucleus to the cytoplasm, increasing its expression and co-localization with NF-κB, thereby suppressing inflammation in PSCs.

3.5. GA inhibits pancreatic fibrosis in vivo via inhibiting YAP1 and NF-κB

To confirm the *in vitro* findings, the anti-fibrosis effects of GA were examined using a dibutyltin dichloride (DBTC)-induced CP model in mice. During the experimental period, mice in the DBTC group exhibited lethargy, decreased activity, and yellowing of their ears, limbs, and tails. Post-mortem examination revealed that DBTC group mice displayed yellowish peritoneal organs and

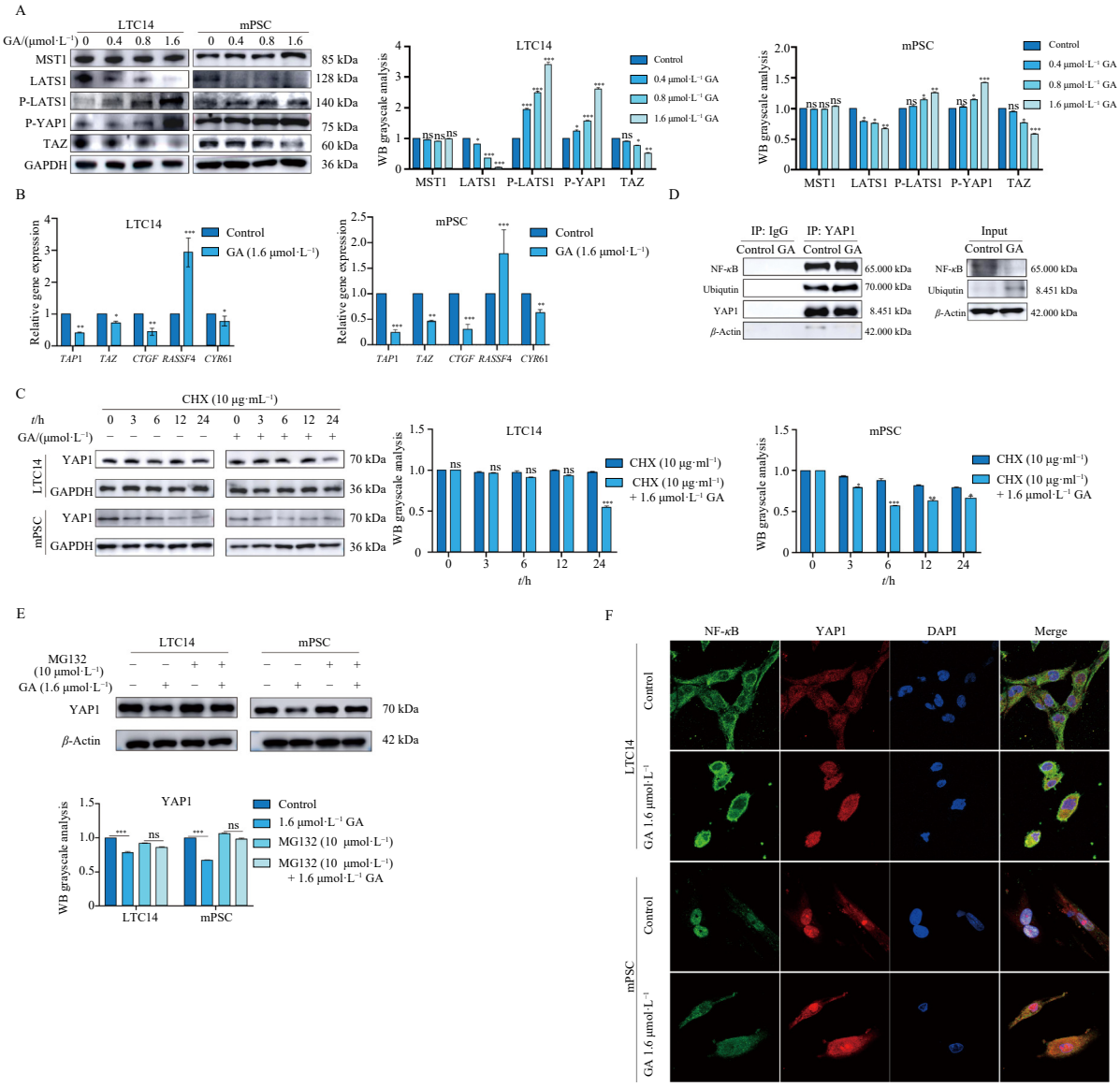

Fig. 4 The effect of GA on the Hippo pathway and the degradation of YAP1. (A) The effect of GA on Hippo pathway-related protein (MST1, LATS1, p-LATS1, p-YAP, and TAZ) in LTC14 and mPSCs was analyzed by Western blot. (B) The effect of GA on mRNA levels of Hippo pathway-related genes (*YAP1*, *TAZ*, *CTGF*, *CYR61* and *RASSF4*) in LTC14 and mPSCs was detected by RT-qPCR. (C) The effect of GA on YAP1 expression in LTC14 and mPSCs without/with 10 μg·mL^{-1} CHX was analyzed by Western blot. (D) The effect of GA on the binding activity between YAP1 and NF-κB/ubiquitin in LTC14 cells was detected by co-immunoprecipitation. (E) The effect of GA on YAP1 expression in LTC14 and mPSCs and the changes in YAP1 after the addition of the proteasome inhibitor MG132 were analyzed by Western blot. (F) The effect of GA on the expression and localization of YAP1 and NF-κB in LTC14 and mPSCs was detected by IF. Data were expressed as mean ± SD (n = 3), $^{*}P < 0.05$, $^{**}P < 0.01$, $^{***}P < 0.001$, $^{****}P < 0.0001$ *vs* control group/specified group.

substantial abdominal fluid accumulation. Analysis of pancreatic tissues demonstrated significant atrophy and yellowing in the DBTC group compared to the control group, while the GA group maintained normal characteristics (Fig. 5A). Serum α-amylase levels exhibited significant variations between the DBTC and GA groups relative to the control group on day 2. However, by day 28, these differences were no longer significant (Fig. 5B). These observations suggest that DBTC administration initially triggered an acute inflammatory response, which progressed to CP by day 28 through repeated inflammatory episodes.

Histological analysis of pancreatic tissue sections using hematoxylin and eosin (H&E) and Masson staining revealed distinct morphological characteristics across groups. The control group demonstrated normal acinar and islet architecture with minimal subcapsular fibrosis and inflammatory cell infiltration. In contrast, the DBTC group exhibited severe pathological changes, including acinar atrophy, reduced islet density, extensive inflammatory infiltration, pronounced fibrosis, macrophage accumulation, and ductal epithelial degeneration. The DBTC + GA treatment group maintained predominantly normal pancreatic architecture, with only isolated regions showing inflammatory infiltration and mild fibrosis in the peripheral pancreatic tissue (Fig. 5C). These observations confirm successful DBTC-induced CP in mice and demonstrate GA's significant inhibitory effect on disease progression. Immunohistochemical analysis Fig. 5D revealed elevated α-SMA protein expression and PSC activation following DBTC administration. Additionally, YAP1 and NF-κB protein levels were elevated compared to controls, suggesting their involvement in pancreatic fibrosis and inflammation. The GA treatment group showed reduced expression of these proteins relative to the DBTC group, indicating that GA potentially inhibits DBTC-induced pancreatic fibrosis through modulation of YAP1 and NF-κB signaling pathways.

4. Discussion

Pancreatic fibrosis is a terminal stage of pancreatitis closely linked to a higher risk of pancreatic cancer [1]. The condition devel-

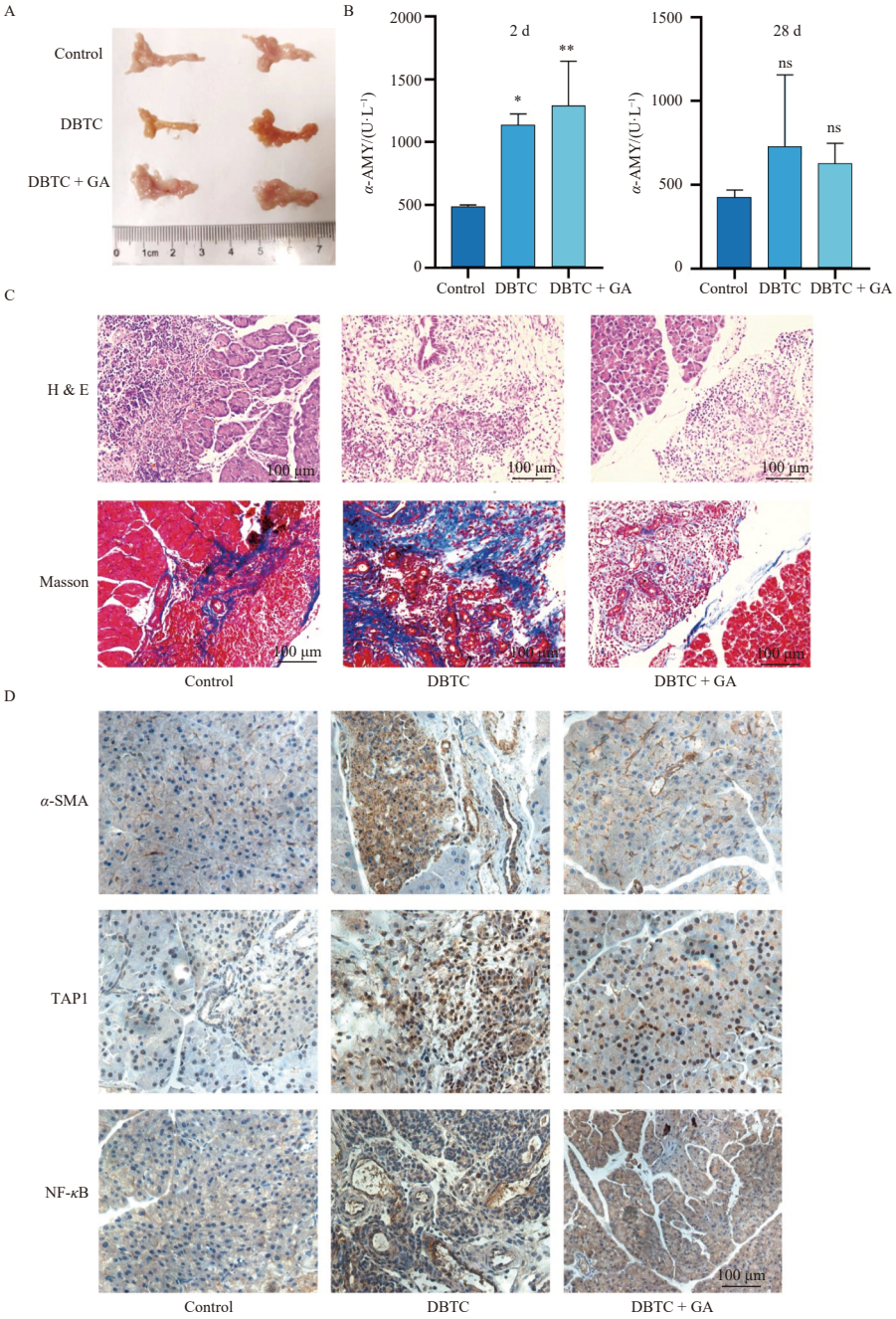

Fig. 5 The effect of GA on pancreatic fibrosis, YAP1, and NF-κB *in vivo*. (A) The DBTC-induced CP model and the effects of GA on pancreatic morphology in mice (n = 6), and representative images were shown. (B) The serum α-amylase levels of mice on days 2 and 28 were measured by ELISA. Data were expressed as mean ± SD (n = 3), $^{*}P < 0.05$, $^{**}P < 0.01$, $^{***}P < 0.001$, $^{****}P < 0.0001$ *vs* control group. (C) The pancreatic sections of different groups of mice were stained by H&E staining and Masson staining (scale bars, 100 μm; n = 6), and representative images were shown. (D) The effect of GA on the expression of α-SMA, YAP1, and NK-κB in pancreatic tissues of mice was detected by immunohistochemistry staining (scale bars, 100 μm; n = 6), and representative images were shown.

ops primarily through pancreatic injury mechanisms, including inflammatory cytokines, growth factors, oxidative stress, and external factors such as alcohol and viral infections, which trigger fibroblast activation and proliferation, ultimately disrupting the balance between ECM production and degradation [7]. PSCs constitute the predominant fibroblast population in pancreatic tissue [10, 43]. Contemporary research establishes PSC activation as a critical event in pancreatic fibrosis progression [8, 12]. Consequently, targeting PSC activation represents a promising therapeutic strategy for preventing and treating pancreatic fibrosis.

GA, a small-molecule compound derived from *Garcinia*, has demonstrated clinical efficacy against various malignancies, including breast cancer, skin cancer, lymphoma, liver cancer, and stomach cancer. Its favorable safety profile and minimal side effects position it as a promising anti-tumor therapeutic agent [32]. The compound exhibits multiple biological activities, including anti-proliferative, anti-inflammatory, anti-metastatic, anti-angiogenic, and anti-oxidant properties [44], suggesting potential anti-fibrotic applications. While previous studies indicate GA's capacity to inhibit fibrosis development [45, 46], its precise mechanism in PSC activation inhibition remains undefined. Our research demonstrates that GA suppresses PSC activation and inflammation through YAP1 inhibition. The compound activates the Hippo pathway and promotes YAP1 cytoplasmic translocation, leading to ubiquitin-mediated degradation, thereby inhibiting PSC activation and fibrosis. This investigation establishes a foundation for developing GA as a therapeutic intervention for pancreatic fibrosis. Experimental findings reveal GA's ability to inhibit proliferation, reduce α-SMA expression, and increase lipid droplets in LTC14 and mPSCs, while preventing TGF-β-induced lipid droplet

reduction. Furthermore, GA decreases expression of inflammation-related proteins (NLRP3, NRF2, IL-6, TNF-α, and NF-κB), reduces collagen I and TIMP1 levels, and enhances MMP2, MMP3, and MMP9 expression. These findings collectively demonstrate GA's robust anti-fibrotic effects through inhibition of LTC14 and mPSC activation and inflammation.

YAP1, a transcription coactivator, plays an essential role in cell proliferation, differentiation, migration, and survival [47, 48]. To investigate whether GA inhibits PSC activation *via* YAP1, YAP1 overexpression cell lines were established. The results demonstrated that GA effectively suppresses PSC activation and inflammatory factor expression by inhibiting YAP1 protein, while simultaneously reducing fibrosis marker protein levels. YAP1 is primarily regulated by the Hippo pathway, whose activation causes YAP1 to bind with TAZ in the cytoplasm, preventing its nuclear translocation and interaction with TEAD proteins [49, 50]. When the Hippo pathway is activated, LATS1 is phosphorylated to p-LATS1, promoting the conversion of YAP1 to p-YAP1. This process leads to YAP1 ubiquitination and degradation, while also inhibiting its nuclear translocation, causing cytoplasmic retention and thus suppressing YAP1 protein function [51, 52]. IF results demonstrated that GA reduces YAP1 nuclear localization and increases its cytoplasmic accumulation. To determine whether GA affects YAP1 expression *via* the Hippo pathway, protein and gene expressions of related factors were analyzed through immunoblotting and qPCR. Results indicated that GA significantly inhibits LATS1 protein expression, increases p-YAP1 levels, and affects downstream gene expression. Preliminary experiments showed that YAP1 converts to p-YAP1 and accumulates in the cytoplasm. Through protein synthesis inhibition and degradation monitoring, GA was found to promote YAP1 degradation. Immunoprecipitation experiments confirmed the binding between YAP1 and NF-κB and increased YAP1-ubiquitin binding, indicating that GA promotes YAP1 ubiquitination and degradation.

Studies indicate that NF-κB serves as a crucial target for treating pancreatic fibrosis. NF-κB is activated early in pancreatitis and regulates inflammation, proliferation, and migration of PSCs [53, 54]. However, the precise mechanisms by which NF-κB contributes to pancreatic fibrosis remain unclear and warrant further investigation. The Hippo-YAP1 pathway exhibits a complex role in the regulation of NF-κB signal transduction. It potentially functions as a regulatory factor of NF-κB signaling. LPS stimulation induces an interaction between YAP and NF-κB subunit p65, suggesting that YAP activation and nuclear translocation are essential for NF-κB activation and TNF-α production [55, 56]. Our results demonstrated that GA reduces the expression of NF-κB and induces YAP1 relocation from the nucleus to the cytoplasm. This mechanism may explain how GA alleviates inflammation in PSCs. IF analysis revealed that GA increases YAP1 co-localization with NF-κB in the cytoplasm. Although GA enhances the interaction between YAP1 and NF-κB, this process occurs in the cytoplasm rather than the nucleus.

GA undergoes complex metabolic processes in the body, including extensive phase I and phase II metabolism facilitated by cytochrome P450 enzymes (CYP450) and phase II enzymes. Given its therapeutic potential, long-term use of GA merits investigation [44]. Preclinical studies in animal models indicate that GA is generally well-tolerated at therapeutic doses [57]. However, potential side effects, including pain, phlebitis, and liver dysfunction have been observed [58, 59]. These effects are dose-dependent at high doses or with prolonged use and can be minimized through appropriate dosing and monitoring [60]. To ensure long-term safety, comprehensive clinical trials are necessary to assess GA's pharmacokinetics, pharmacodynamics, and toxicological profile.

5. Conclusions

In conclusion, GA inhibits PSC proliferation, modulates their lipid metabolism and inflammatory responses, and suppresses their activation through YAP1 inhibition. By activating the Hippo signaling pathway, GA impedes YAP1 nuclear translocation, facilitates its degradation, and attenuates the progression of pancreatic fibrosis. These findings demonstrate the antifibrotic efficacy of GA and provide a mechanistic foundation for its potential clinical application as a therapeutic agent in the treatment of pancreatic fibrosis.

Funding

This work was supported by the Fundamental Research Funds for the Central Universities (No. 2632024TD07).

Supporting information

Supporting information for this work can be obtained by contacting the corresponding authors *via* E-mail.

Conflict of interest

The authors declare no conflict of interest.

References

1 Beyer G, Habtezion A, Werner J, et al. Chronic pancreatitis. *Lancet*. 2020;396 (10249):499-512. https://doi.org/10.1016/S0140-6736(20)31318-0.
2 Vege SS, Chari ST. Chronic pancreatitis. *N Engl J Med*. 2022;386(9):869-878. https://doi.org/10.1056/NEJMcp1809396.
3 Dib B. A study of intrathecal self-injection of morphine by rats, and the difficulties entailed. *Pain*. 1985;23(2):177-185. https://doi.org/10.1016/0304-3959(85)90058-2.
4 Zhang W, Zhang S, Zhang W, et al. Matrix stiffness and its influence on pancreatic diseases. *Biochim Biophys Acta Rev Cancer*. 2021;1876(1):188583. https://doi.org/10.1016/j.bbcan.2021.188583.
5 An J, Jiang T, Qi L, et al. Acinar cells and the development of pancreatic fibrosis. *Cytokine Growth Factor Rev*. 2023;71-72:40-53. https://doi.org/10.1016/j.cytogfr.2023.05.003.
6 Thomas D, Radhakrishnan P. Tumor-stromal crosstalk in pancreatic cancer and tissue fibrosis. *Mol Cancer*. 2019;18(1):14. https://doi.org/10.1186/s12943-018-0927-5.
7 Baer JM, Zuo C, Kang L, et al. Fibrosis induced by resident macrophages has divergent roles in pancreas inflammatory injury and PDAC. *Nat Immunol*. 2023;24(9):1443-1457. https://doi.org/10.1038/s41590-023-01579-x.
8 Schnittert J, Bansal R, Prakash J. Targeting pancreatic stellate cells in cancer. *Trends Cancer*. 2019;5(2):128-142. https://doi.org/10.1016/j.trecan.2019.01.001.
9 Wang Y, Chen K, Liu G, et al. Disruption of super-enhancers in activated pancreatic stellate cells facilitates chemotherapy and immunotherapy in pancreatic cancer. *Adv Sci (Weinh)*. 2024;11(16):e2308637. https://doi.org/10.1002/advs.202308637.
10 Wang D, Han S, Lv G, et al. Pancreatic acinar cells-derived sphingosine-1-phosphate contributes to fibrosis of chronic pancreatitis *via* inducing autophagy and activation of pancreatic stellate cells. *Gastroenterology*. 2023;165(6):1488-1504.e20. https://doi.org/10.1053/j.gastro.2023.08.029.
11 Sarkar R, Xu Z, Perera CJ, et al. Emerging role of pancreatic stellate cell-derived extracellular vesicles in pancreatic cancer. *Semin Cancer Biol*. 2023;93:114-122. https://doi.org/10.1016/j.semcancer.2023.05.007.
12 Yang X, Chen J, Wang J, et al. Very-low-density lipoprotein receptor-enhanced lipid metabolism in pancreatic stellate cells promotes pancreatic fibrosis. *Immunity*. 2022;55(7):1185-1199.e8. https://doi.org/10.1016/j.immuni.2022.06.001.
13 Wu Y, Zhang C, Guo M, et al. Targeting pancreatic stellate cells in chronic pancreatitis: focus on therapeutic drugs and natural compounds. *Front Pharmacol*. 2022;13:1042651. https://doi.org/10.3389/fphar.2022.1042651.
14 Huang C, Iovanna J, Santofimia-Castaño P. Targeting fibrosis: the bridge that connects pancreatitis and pancreatic cancer. *Int J Mol Sci*. 2021;22(9):4970. https://doi.org/10.3390/ijms22094970.
15 Sherman MH. Stellate cells in tissue repair, inflammation, and cancer. *Annu Rev Cell Dev Biol*. 2018;34:333-355. https://doi.org/10.1146/annurev-cellbio-100617-062855.
16 Ramakrishnan P, Loh WM, Gopinath SCB, et al. Selective phytochemicals targeting pancreatic stellate cells as new anti-fibrotic agents for chronic pancreatitis and pancreatic cancer. *Acta Pharm Sin B*. 2020;10(3):399-413. https://doi.org/10.1016/j.apsb.2019.11.008.
17 Li W, Sun L, Lei J, et al. Curcumin inhibits pancreatic cancer cell invasion and EMT by interfering with tumor-stromal crosstalk under hypoxic conditions *via* the IL-6/ERK/NF-κB axis. *Oncol Rep*. 2020;44(1):382-392. https://doi.org/10.3892/or.2020.7600.
18 Zeng XP, Zeng JH, Lin X, et al. Puerarin ameliorates caerulein-induced chronic pancreatitis *via* inhibition of MAPK signaling pathway. *Front Pharmacol*. 2021;12:686992. https://doi.org/10.3389/fphar.2021.686992.

19 Garg B, Giri B, Modi S, et al. NFκB in pancreatic stellate cells reduces infiltration of tumors by cytotoxic T cells and killing of cancer cells, *via* up-regulation of CXCL12. *Gastroenterology*. 2018;155(3):880-891.e8. https://doi.org/10.1053/j.gastro.2018.05.051.

20 Zhao T, Xiao D, Jin F, et al. ESE3-positive PSCs drive pancreatic cancer fibrosis, chemoresistance and poor prognosis *via* tumour-stromal IL-1β/NF-κB/ESE3 signalling axis. *Br J Cancer*. 2022;127(8):1461-1472. https://doi.org/10.1038/s41416-022-01927-y.

21 Wu N, Xu XF, Xin JQ, et al. The effects of nuclear factor-kappa B in pancreatic stellate cells on inflammation and fibrosis of chronic pancreatitis. *J Cell Mol Med*. 2021;25(4):2213-2227. https://doi.org/10.1111/jcmm.16213.

22 Morvaridi S, Dhall D, Greene MI, et al. Role of YAP and TAZ in pancreatic ductal adenocarcinoma and in stellate cells associated with cancer and chronic pancreatitis. *Sci Rep*. 2015;5:16759. https://doi.org/10.1038/srep16759.

23 Wu Y, Aegerter P, Nipper M, et al. Hippo signaling pathway in pancreas development. *Front Cell Dev Biol*. 2021;9:663906. https://doi.org/10.3389/fcell.2021.663906.

24 Tanaka HY, Nakazawa T, Miyazaki T, et al. Targeting ROCK2 improves macromolecular permeability in a 3D fibrotic pancreatic cancer microenvironment model. *J Control Release*. 2024;369:283-295. https://doi.org/10.1016/j.jconrel.2024.03.041.

25 Cortes E, Sarper M, Robinson B, et al. GPER is a mechanoregulator of pancreatic stellate cells and the tumor microenvironment. *EMBO Rep*. 2019;20(1):e46556. https://doi.org/10.15252/embr.201846556.

26 Xiao Y, Zhang H, Ma Q, et al. YAP1-mediated pancreatic stellate cell activation inhibits pancreatic cancer cell proliferation. *Cancer Lett*. 2019;462:51-60. https://doi.org/10.1016/j.canlet.2019.07.015.

27 Yuan Y, Li Z, Li M, et al. Mitochondria oxidative stress mediated nicotine-promoted activation of pancreatic stellate cells by regulating mitochondrial dynamics. *Toxicol In Vitro*. 2022;84:105436. https://doi.org/10.1016/j.tiv.2022.105436.

28 Xue R, Wang J, Yang L, et al. Coenzyme Q10 ameliorates pancreatic fibrosis *via* the ROS-triggered mTOR signaling pathway. *Oxid Med Cell Longev*. 2019;2019:8039694. https://doi.org/10.1155/2019/8039694.

29 Ryu GR, Lee E, Chun HJ, et al. Oxidative stress plays a role in high glucose-induced activation of pancreatic stellate cells. *Biochem Biophys Res Commun*. 2013;439(2):258-263. https://doi.org/10.1016/j.bbrc.2013.08.046.

30 Dey A, Varelas X, Guan KL. Targeting the Hippo pathway in cancer, fibrosis, wound healing and regenerative medicine. *Nat Rev Drug Discov*. 2020;19(7):480-494. https://doi.org/10.1038/s41573-020-0070-z.

31 Ryan MB, Der CJ, Wang-Gillam A, et al. Targeting RAS-mutant cancers: is ERK the key? *Trends Cancer*. 2015;1(3):183-198. https://doi.org/10.1016/j.trecan.2015.10.001.

32 O'Neil BH, Scott AJ, Ma WW, et al. A phase II/III randomized study to compare the efficacy and safety of rigosertib plus gemcitabine versus gemcitabine alone in patients with previously untreated metastatic pancreatic cancer. *Ann Oncol*. 2015;26(9):1923-1929. https://doi.org/10.1093/annonc/mdv264.

33 Yu Z, Jv Y, Cai L, et al. Gambogic acid attenuates liver fibrosis by inhibiting the PI3K/AKT and MAPK signaling pathways *via* inhibiting HSP90. *Toxicol Appl Pharmacol*. 2019;371:63-73. https://doi.org/10.1016/j.taap.2019.03.028.

34 Wang L, Li S, Yao Y, et al. The role of natural products in the prevention and treatment of pulmonary fibrosis: a review. *Food Funct*. 2021;12(3):990-1007. https://doi.org/10.1039/D0FO03001E.

35 Xu Y, Zhang X, Zhang R, et al. AFP deletion leads to anti-tumorigenic but pro-metastatic roles in liver cancers with concomitant CTNNB1 mutations. *Cancer Lett*. 2023;566:216240. https://doi.org/10.1016/j.canlet.2023.216240.

36 Kumar K, DeCant BT, Grippo PJ, et al. BET inhibitors block pancreatic stellate cell collagen I production and attenuate fibrosis *in vivo*. *JCI Insight*. 2017;2(3):e88032. https://doi.org/10.1172/jci.insight.88032.

37 Bhattacharjee S, Hamberger F, Ravichandra A, et al. Tumor restriction by type I collagen opposes tumor-promoting effects of cancer-associated fibroblasts. *J Clin Invest*. 2021;131(11):e146987. https://doi.org/10.1172/JCI146987.

38 Kapoor A, Yao W, Ying H, et al. Yap1 activation enables bypass of oncogenic kras addiction in pancreatic cancer. *Cell*. 2019;179(5):1239. https://doi.org/10.1016/j.cell.2019.10.037.

39 Liu M, Zhang Y, Yang J, et al. Zinc-dependent regulation of ZEB1 and YAP1 coactivation promotes epithelial-mesenchymal transition plasticity and metastasis in pancreatic cancer. *Gastroenterology*. 2021;160(5):1771-1783.e1. https://doi.org/10.1053/j.gastro.2020.12.077.

40 Mooring M, Fowl BH, Lum SZC, et al. Hepatocyte stress increases expression of yes-associated protein and transcriptional coactivator with PDZ-binding motif in hepatocytes to promote parenchymal inflammation and fibrosis. *Hepatology*. 2020;71(5):1813-1830. https://doi.org/10.1002/hep.30928.

41 Hong AW, Meng Z, Yuan HX, et al. Osmotic stress-induced phosphorylation by NLK at Ser128 activates YAP. *EMBO Rep*. 2017;18(1):72-86. https://doi.org/10.15252/embr.201642681.

42 Ni W, Yao S, Zhou Y, et al. Long noncoding RNA GAS5 inhibits progression of colorectal cancer by interacting with and triggering YAP phosphorylation and degradation and is negatively regulated by the m(6)A reader YTHDF3. *Mol Cancer*. 2019;18(1):143. https://doi.org/10.1186/s12943-019-1079-y.

43 Pothula SP, Xu Z, Goldstein D, et al. Key role of pancreatic stellate cells in pancreatic cancer. *Cancer Lett*. 2016;381(1):194-200. https://doi.org/10.1016/j.canlet.2015.10.035.

44 Hatami E, Jaggi M, Chauhan SC, et al. Gambogic acid: a shining natural compound to nanomedicine for cancer therapeutics. *Biochim Biophys Acta Rev Cancer*. 2020;1874(1):188381. https://doi.org/10.1016/j.bbcan.2020.188381.

45 Qu Y, Zhang G, Ji Y, et al. Protective role of gambogic acid in experimental pulmonary fibrosis *in vitro* and *in vivo*. *Phytomedicine*. 2016;23(4):350-358. https://doi.org/10.1016/j.phymed.2016.01.011.

46 Tao S, Yang L, Wu C, et al. Gambogenic acid alleviates kidney fibrosis *via* epigenetic inhibition of EZH2 to regulate Smad7-dependent mechanism. *Phytomedicine*. 2022;106:154390. https://doi.org/10.1016/j.phymed.2022.154390.

47 Liu Y, Lu T, Zhang C, et al. Activation of YAP attenuates hepatic damage and fibrosis in liver ischemia-reperfusion injury. *J Hepatol*. 2019;71(4):719-730. https://doi.org/10.1016/j.jhep.2019.05.029.

48 Franklin JM, Wu Z, Guan KL. Insights into recent findings and clinical application of YAP and TAZ in cancer. *Nat Rev Cancer*. 2023;23(8):512-525. https://doi.org/10.1038/s41568-023-00579-1.

49 Liu J, Bai W, Zhou T, et al. SDCBP promotes pancreatic cancer progression by preventing YAP1 from *β*-TrCP-mediated proteasomal degradation. *Gut*. 2023;72(9):1722-1737. https://doi.org/10.1136/gutjnl-2022-327492.

50 Guo Y, Cui Y, Li Y, et al. Cytoplasmic YAP1-mediated ESCRT-III assembly promotes autophagic cell death and is ubiquitinated by NEDD4L in breast cancer. *Cancer Commun (Lond)*. 2023;43(5):582-612. https://doi.org/10.1002/cac2.12417.

51 Ibar C, Irvine KD. Integration of Hippo-YAP signaling with metabolism. *Dev Cell*. 2020;54(2):256-267. https://doi.org/10.1016/j.devcel.2020.06.025.

52 Wang T, Wang D, Sun Y, et al. Regulation of the Hippo/YAP axis by CXCR7 in the tumorigenesis of gastric cancer. *J Exp Clin Cancer Res*. 2023;42(1):297. https://doi.org/10.1186/s13046-023-02870-3.

53 Bordeleau F, Mason BN, Lollis EM, et al. Matrix stiffening promotes a tumor vasculature phenotype. *Proc Natl Acad Sci U S A*. 2017;114(3):492-497. https://doi.org/10.1073/pnas.1613855114.

54 Wu Y, Zhang C, Jiang K, et al. The role of stellate cells in pancreatic ductal adenocarcinoma: targeting perspectives. *Front Oncol*. 2020;10:621937. https://doi.org/10.3389/fonc.2020.621937.

55 Yang K, Xu J, Fan M, et al. Lactate suppresses macrophage pro-inflammatory response to LPS stimulation by inhibition of YAP and NF-κB activation *via* GPR81-mediated signaling. *Front Immunol*. 2020;11:587913. https://doi.org/10.3389/fimmu.2020.587913.

56 LaCanna R, Liccardo D, Zhang P, et al. Yap/Taz regulate alveolar regeneration and resolution of lung inflammation. *J Clin Invest*. 2019;129(5):2107-2122. https://doi.org/10.1172/JCI125014.

57 Banik K, Harsha C, Bordoloi D, et al. Therapeutic potential of gambogic acid, a caged xanthone, to target cancer. *Cancer Lett*. 2018;416:75-86. https://doi.org/10.1016/j.canlet.2017.12.014.

58 Qi Q, You Q, Gu H, et al. Studies on the toxicity of gambogic acid in rats. *J Ethnopharmacol*. 2008;117(3):433-438. https://doi.org/10.1016/j.jep.2008.02.027.

59 Zhang D, Wang W, Hou T, et al. New delivery route of gambogic acid *via* skin for topical targeted therapy of cutaneous melanoma and reduction of systemic toxicity. *J Pharm Sci*. 2021;110(5):2167-2176. https://doi.org/10.1016/j.xphs.2020.12.024.

60 Jiang LL, Li K, Lin QH, et al. Gambogic acid causes fin developmental defect in zebrafish embryo partially *via* retinoic acid signaling. *Reprod Toxicol*. 2016;63:161-168. https://doi.org/10.1016/j.reprotox.2016.06.004.